

## Article

# Four Thermochromic *o*-Hydroxy Schiff Bases of $\alpha$ -Aminodiphenylmethane: Solution and Solid State Study

Marija Zbačnik <sup>1,\*</sup>, Katarina Pičuljan <sup>1</sup>, Jelena Parlov-Vuković <sup>2</sup>, Predrag Novak <sup>1</sup> and Andreas Roodt <sup>3</sup>

<sup>1</sup> Department of Chemistry, Faculty of Science, University of Zagreb, Horvatovac 102a, HR-10000 Zagreb, Croatia; kpiculjan@chem.pmf.hr (K.P.); pnovak@chem.pmf.hr (P.N.)

<sup>2</sup> Refining and Marketing Development Sector, Central Testing Laboratory Department, INA Industrija nafte, d.d., Lovinčičeva 4, HR-10000 Zagreb, Croatia; Jelena.Parlov-Vukovic@ina.hr

<sup>3</sup> Department of Chemistry, University of the Free State, Bloemfontein 9301, South Africa; RoodtA@ufs.ac.za

\* Correspondence: mzbacnik@chem.pmf.hr; Tel.: +385-1-4606-379

Academic Editor: Johan Wouters

Received: 15 December 2016; Accepted: 11 January 2017; Published: 14 January 2017

**Abstract:** More than a hundred years after the first studies of the photo- and thermochromism of *o*-hydroxy Schiff bases (imines), it is still an intriguing topic that fascinates several research groups around the world. The reasons for such behavior are still under investigation, and this work is a part of it. We report the solution-based and mechanochemical synthesis of four *o*-hydroxy imines derived from  $\alpha$ -aminodiphenylmethane. The thermochromic properties were studied for the single crystal and polycrystalline samples of the imines. The supramolecular impact on the keto-enol tautomerism in the solid state was studied using SCXRD and NMR, while NMR spectroscopy was used for the solution state. All four imines are thermochromic, although the color changes of the single crystals are not as strong as of the polycrystalline samples. One of the imines shows negative thermochromism, and that one is in keto-amine tautomeric form, both in the solid state as in solution.

**Keywords:** thermochromism; Schiff base; keto-enol tautomerism; solution-based synthesis; mechanosynthesis

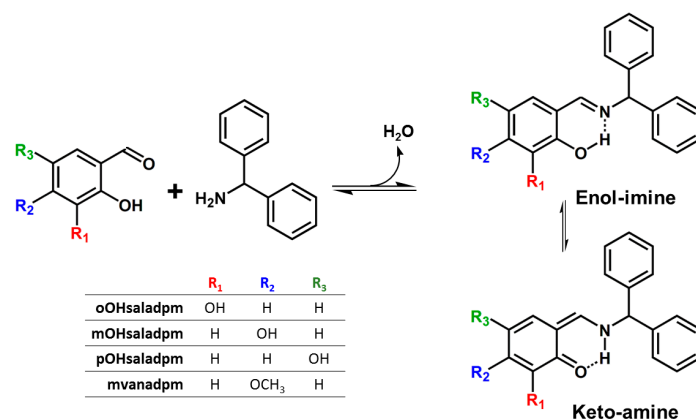
## 1. Introduction

There is nothing more beautiful and at the same time intriguing to the eye of a chemist than a color change upon a change in the environment. That is one of the reasons why numerous scientific groups have been studying thermo- and/or photochromism for more than 100 years [1–4]. The continuous interest in such properties in the solid state is to understand the origin of the chromic behavior, but moreover to use crystal engineering to manipulate or control their physico-chemical properties to design materials with better performance [5–11].

Among many compounds that exhibit thermo- and/or photochromism in the solid state, *o*-hydroxy aromatic imines or Schiff bases have been drawing special attention for a long time. *N*-substituted imines can be easily synthesized by condensation of aldehydes (or ketones) and primary amines [12] and used not only for the investigation of their physico-chemical properties, but also because of their well-recognized biological and pharmacological properties [9,13–16], as well as their metal complexes [17]. There are three mutually-dependent reasons for such behavior in the solid state described in the literature: (a) proton transfer via intramolecular O $\cdots$ N hydrogen bonds and thus (b) the change of the tautomeric form [18–23] and (c) the contribution of fluorescence and not only of light absorption as a consequence of the tautomeric change and the change in molecular geometry [24]. Another intriguing “well-known fact” about thermo- and/or photochromism of *o*-hydroxy Schiff bases is that these two phenomena are mutually exclusive and that imines with planar molecules

(dihedral angle between aromatic subunits  $\phi < 25^\circ$ ) should be thermochromic and ones with non-planar molecules ( $\phi > 25^\circ$ ) should be photochromic [18–21]. The above-mentioned reasons and facts are the motives why scientists are still trying to either reaffirm them or to find *o*-hydroxy imines in which these reasons cannot be strictly determined, but the imines do show such a chromic change [22–32]. It should be pointed out that the empirical rule on the molecular (non)planarity should not be applied to *o*-hydroxy Schiff bases obtained from benzylamine derivatives and aliphatic amines, as stated before in the literature [25,26,28,30]. This group of *o*-hydroxy imines have a –CH– group as a spacer between the imine nitrogen atom and the aromatic ring, and thus, the electronic conjugation is disrupted, meaning that the electron density on the imine N-atom is crucial to thermochromism. On the other hand, the research of prosperous methods of synthesis, such as mechanochemical ones, provides new insights into faster and ecologically and economically more acceptable ways to prepare new, but also already known compounds [33]. Various Schiff bases have been obtained in such a manner by neat (NG), liquid-assisted (LAG) and seeding-assisted (SEAG) grinding [30–32,34–36].

Herein, we report solvent-free and solution-based syntheses of four *o*-hydroxy Schiff bases obtained from salicylaldehyde derivatives (*o*-, *m*- and *p*-hydroxy salicylaldehyde, **oOHsal**, **mOHsal**, **pOHsal**, and *m*-vanillin, **mvn**) and  $\alpha$ -aminodiphenylmethane (**adpm**), as well as the investigation of their thermochromic properties. The effectiveness of the used synthetic method was studied by means of PXRD, DSC and TG analyses. Their thermochromic properties were checked by repeated exposure to temperature change from room to liquid-nitrogen temperature. The supramolecular impact on the keto-enol tautomerism (Scheme 1) was studied using SCXRD and solution and solid-state NMR spectroscopy.



**Scheme 1.** View of molecular structures and keto-enol tautomeric equilibrium of four *o*-hydroxy imines derived from  $\alpha$ -aminodiphenylmethane. **sal**, salicylaldehyde; **adpm**, aminodiphenylmethane; **mvn**, *m*-vanillin.

Multinuclear ( $^1\text{H}$ ,  $^{13}\text{C}$ ,  $^{15}\text{N}$ ) NMR spectroscopy is the most commonly-used experimental method to study keto-enol tautomeric equilibrium in *ortho*-hydroxy Schiff bases [37–41]. The nitrogen chemical shift,  $\delta\text{N}$ , is very sensitive to intramolecular proton transfer and therefore to the change in the tautomeric equilibrium in *o*-hydroxy Schiff bases. The keto-enol tautomerism is characterized by the protonation of the imine nitrogen leading to a large upfield shift of the nitrogen signal, for more than 100 ppm. A typical  $\delta\text{N}$  value for pure OH-form, without the intramolecular O–H...N H-bond, is approximately 330 ppm (referenced to the  $\text{NH}_3(\text{l})$ ). The existence of intramolecular hydrogen bonds shifts the imine nitrogen signal upfield to a value of about 280 ppm, characteristic for OH-forms with localized intramolecular O–H...N hydrogen bonds. Stronger hydrogen bonds and/or the proton transfer from the parent hydroxyl oxygen to the imine nitrogen atom causes a further  $\delta\text{N}$  upfield shift.  $\delta\text{N}$  values lower than 180 ppm (to 140 ppm) are characteristic for pure NH-forms. In general, the proton transfer from an oxygen to a nitrogen atom results in nitrogen signal upfield shift and carbon

C2 signal downfield shift (higher  $\delta\text{C2}$  value). Typical  $\delta\text{C2}$  values are about 150 ppm for pure OH-form and about 180 ppm for pure NH-form, but these are strongly influenced by the nature of aryl ring substituents in *ortho*-hydroxy Schiff bases. In addition to  $\delta\text{N}$  and  $\delta\text{C2}$ , the chemical shift of the OH/NH proton,  $\delta\text{XH}$ , is qualitative evidence for the presence of intramolecular O $\cdots$ H $\cdots$ N hydrogen bonds in *ortho*-hydroxy imines. Generally, the protons that participate in intramolecular H-bonds show higher values of chemical shifts compared to the structures without the intramolecular H-bond. However, it is not possible to define the exact position of the protons in H-bonds only on the basis of the  $\delta\text{XH}$  value. In *ortho*-hydroxy Schiff bases, the  $\delta\text{XH}$  values were observed in the range 7–18 ppm; values in the range 12–18 ppm strongly indicate the presence of intramolecular O $\cdots$ H $\cdots$ N hydrogen bond.

## 2. Results and Discussion

### 2.1. Syntheses

In all four cases, a 1 mmol:1 mmol stoichiometric ratio of aldehyde and amine was used in order to obtain the Schiff base. Syntheses were performed at room temperature (25 °C) and at 40%–60% relative humidity. Bulk products of syntheses and recrystallization were characterized by means of PXRD, DSC and TGA (Figures C1–C5) and solution and solid state NMR. The systematic names and acronyms of the compounds are listed in Table A2, while the details on synthetic procedures are given in Appendix B. Photographs of the grinding experiments and the results of the PXRD experiments are shown in Figure 1.

Mechanochemical syntheses of all four imines reported here were successful. There are no diffraction maxima of the used aldehydes in the PXRD patterns, indicating that the imines were obtained as pure crystalline phases. Neat grinding (NG) of **oOHsal** and **adpm** in an agate mortar leads first to an orange moist paste-like reaction mixture, which starts to solidify after 2 min. An orange powder identified as **oOHsaladpm** was obtained in 6 min of grinding. The conversion to **oOHsaladpm** by grinding was complete according to the PXRD patterns, and the data are in good agreement with the bulk obtained from chloroform. A yellow paste-like mixture stable for 10 min was obtained by means NG of **mOHsal** and **adpm**. The mixture then starts to solidify giving a yellow powder product in 16 min from the start. Mechanochemical synthesis of **mOHsaladpm** was complete, and the PXRD data of the powder product are in good agreement with the data of the bulk material obtained by crystallization experiments using acetone. NG of equimolar quantities of **pOHsal** and **adpm** afforded an orange paste, which converts to an orange powder product in 13 min. The conversion to **pOHsaladpm** was complete as revealed by PXRD experiments, and the diffraction maxima are in good agreement with the maxima of the bulk obtained by crystallization experiment using EtOH. The **mvanadpm** was obtained in quantitative yield by NG for 3 min as a yellowish-green powder, which gradually changes its color to light-yellow in 30 min. PXRD data of both obtained materials are in good agreement with the corresponding bulk obtained by crystallization experiments using ethanol.

The solution-based syntheses were performed according to the detailed procedures given in Appendix B in order to obtain single crystals by slow evaporation of solvent for structure analysis by means of SCXRD. The aldehydes (1 mmol) were dissolved in suitable solvents, and **adpm** (1 mmol) was added to the solution. The vial was then left semi-closed at RT for the solvent to evaporate. PXRD data were collected after solvent evaporation (Figure 1).

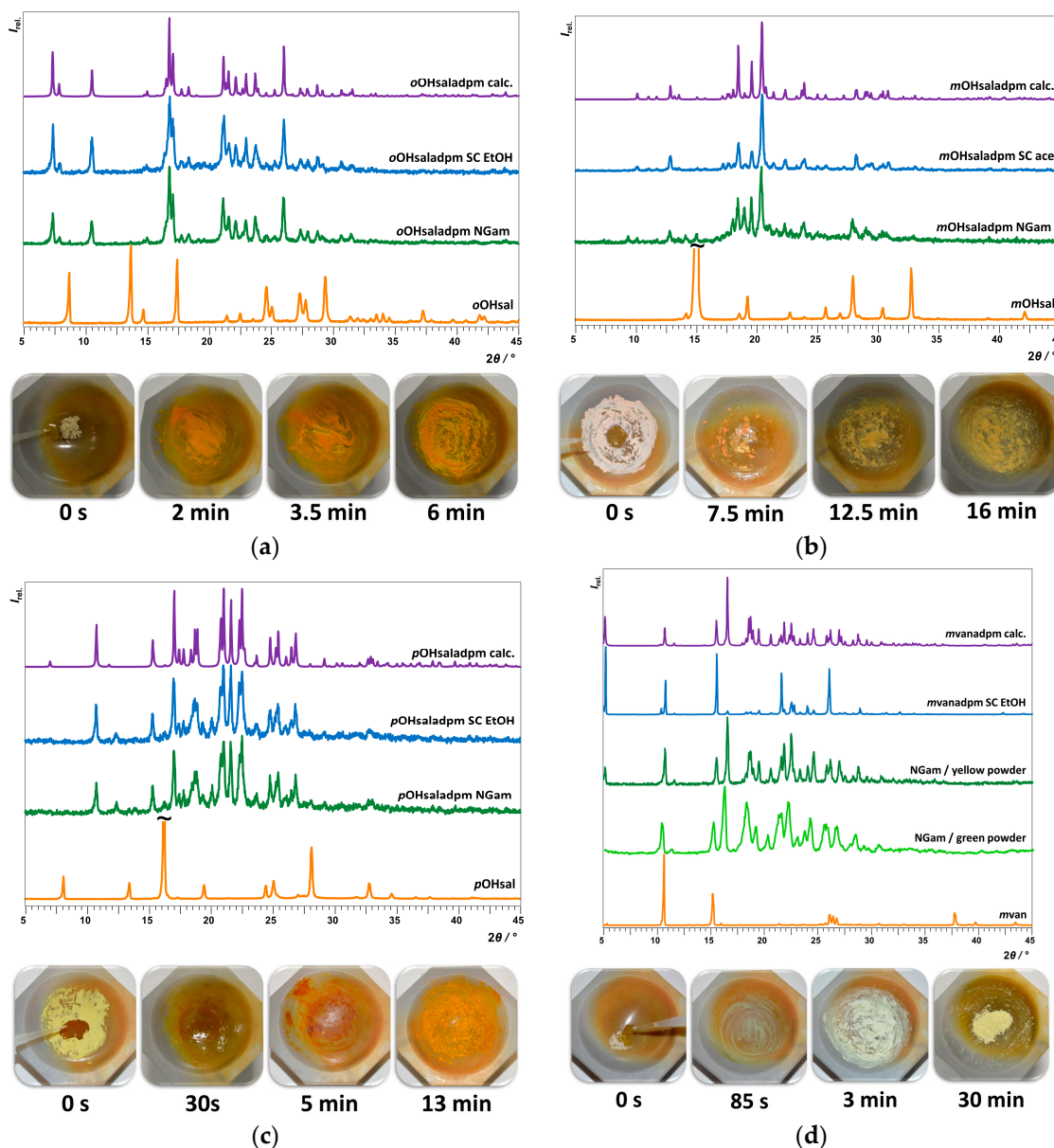


**Figure 1.** PXRD patterns of aldehydes and products of mechanochemical- and solution-based syntheses along with the calculated patterns (top) and photographs of the grinding experiments (bottom) for (a) *o*OHsaladpm; (b) *m*OHsaladpm; (c) *p*OHsaladpm and (d) *m*vanadpm.

## 2.2. Structural Analysis and Thermochromism

General and crystallographic data for all compounds and hydrogen bond geometry data are given in Appendix B, Tables B1–B6. Thermal ellipsoid plots showing the atom-labelling schemes are given in Figure B1, while the electron density maps are presented in Figure B2. Packing diagrams are shown in Figures B3–B5.

The thermochromic properties of the imines were checked by repeated exposure to a temperature change from room to liquid-nitrogen temperature. The samples of powder products were put in test tubes and submerged repeatedly into liquid nitrogen (77 K), while the thermochromism of the single crystals was studied at 298 K and 150 K. The results are presented in Figure 2, showing that all four imines show reversible thermochromism. *m*OHsaladpm shows negative thermochromism (Figure 2b), which is rare, although the same phenomenon was reported for the Schiff base derived from salicylaldehyde and *adpm* [30]. The color of the *m*OHsaladpm crystal changes from light yellow



to yellow upon cooling to 150 K, while the powder becomes pale orange at 77 K. The color of the crystal of **pOHsaladpm** does not differ considerably by cooling from 298 K down to 150 K, but the color of the powder sample changes from brownish-orange to yellow by cooling to 77 K. A small structural change, e.g., the position of a hydroxy group or a change to a methoxy group on the aldehyde moiety, was shown to be a good strategy for the design of new thermochromic Schiff bases.

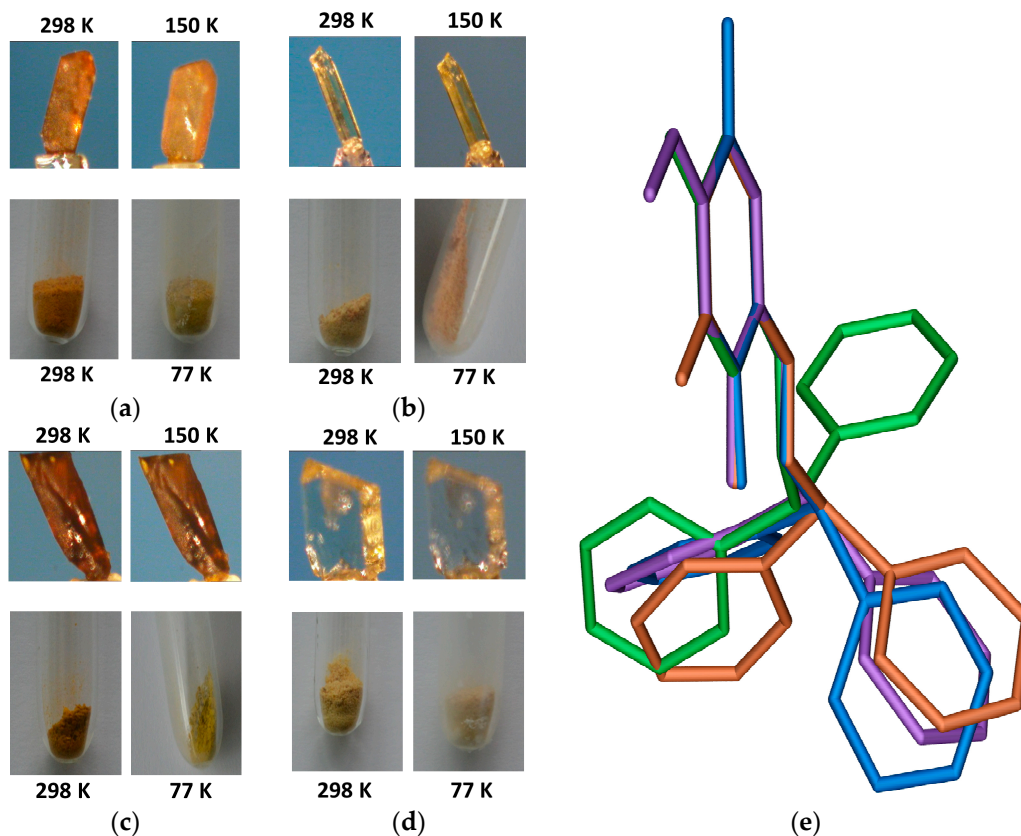


**Figure 2.** Photographs of single crystals and grinding products of (a) **oOHsaladpm**, (b) **mOHsaladpm**, (c) **pOHsaladpm** and (d) **mvnadpm** at 298, 150 and 77 K and (e) the view of the molecular overlay of **oOHsaladpm** (orange), **mOHsaladpm** (green), **pOHsaladpm** (blue) and **mvnadpm** (violet).

Single crystal X-ray analysis of the four imines showed that there are conformational differences in their molecules (Figure 2e). The molecular overlay and dihedral angles between the aromatic rings being from  $45^{\circ}$ – $90^{\circ}$  (Table B2) illustrate the deviation from the planarity of the molecules, although one should take into consideration that all of them are actually benzylamine derivatives and thus contain a  $-\text{CH}-$  group as a spacer between the imine N-atom and the aromatic subunits [25,26,30]. The tautomer present in the solid state was determined according to the C2–O1 and C7–N1 bond length criterion (Table B2), and the position of the hydrogen atom (H1) was located from the electron density map (Figure B2).

**oOHsaladpm** crystallizes in the  $P\bar{1}$  space group of the triclinic system with two molecules per unit cell. The molecules are found to be in enol-imine tautomeric form connected via O2–H2...O1 and weak C10–H10...O2 (Table B3) into discrete centrosymmetric dimers (Figure 3a). There are no other significant interactions in the crystal structure of **oOHsaladpm**, since the shortest one is actually C17–H17... $\pi$  (C11–C12) of 3.635 Å in length. The fingerprint plot of **oOHsaladpm** shows that the crystal packing is governed by H...H (54%) and C...H (33%) intermolecular contacts (Figure 3b). The packing diagram of **oOHsaladpm** molecules is shown in Figure B3.

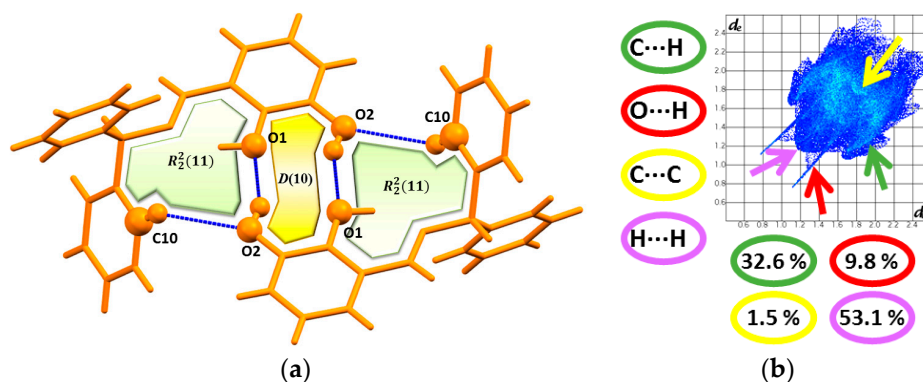


**Figure 3.** View of (a) a centrosymmetric dimer of **oOHsaladpm** molecules formed by means of O–H...O and C–H...O interactions and (b) the 2D-fingerprint plot with marked corresponding regions: green arrow for C...H contacts, red arrows for O...H contacts, yellow arrow for C...C contacts and violet arrow for H...H contacts.

**mOHsaladpm** crystallizes in the  $P2_1/c$  space group of the monoclinic system with four molecules per unit cell. The molecules are found to be in the keto-amine tautomeric form, and the O1 atom is a tetrafurcated acceptor of intermolecular hydrogen bonds. The molecules are connected via O2–H2...O1 and three C–H...O (Table B4, Figure 4a) into a network (Figure B4). The intermolecular O2–H2...O1 and C3–H3...O1 interactions between the molecules of **mOHsaladpm** are shorter than the intramolecular N1–H1...O1 hydrogen bond; thus, supramolecular influence on the proton transfer from the parent O1 atom to the N1 atom is facilitated in the solid state [32]. The fingerprint plot of **mOHsaladpm** shows that the crystal packing is directed by H...H (51%) and C...H (32%) intermolecular contacts, but it should be stated that the percentage of the O...H (15%) contacts in this compound is bigger than in other ones reported here (Figure 4b).

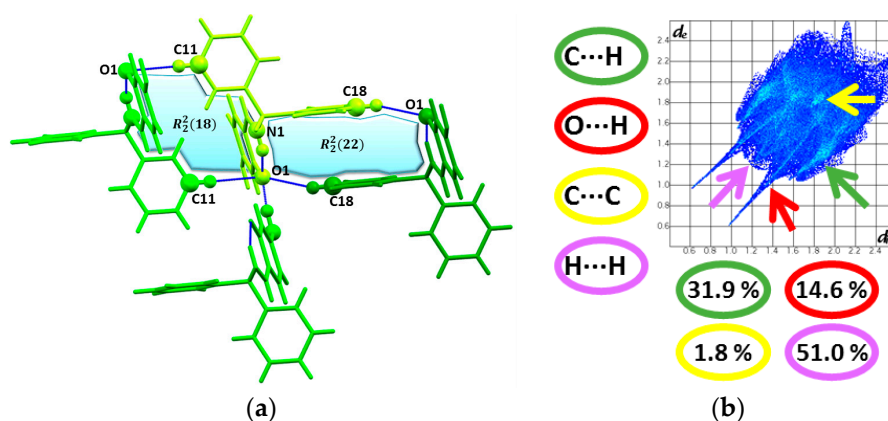


**Figure 4.** View of (a) a tetramer of **mOHsaladpm** molecules formed by means of O–H...O and C–H...O interactions and (b) the 2D-fingerprint plot with marked corresponding regions: green arrow for C...H contacts, red arrows for O...H contacts, yellow arrow for C...C contacts and violet arrow for H...H contacts.

**pOHsaladpm** crystallizes in the  $P2_1/c$  space group of monoclinic system with four molecules per unit cell. The molecules are found to be in enol-imine tautomeric form. Two chains of the molecules of **pOHsaladpm** spread via [010] and [001] direction forming sheets (Table B5, Figure 5a) by means of O2–H2...O1, C13–H13... $\pi$  (3.62 Å) and C3–H3...O1 contacts, respectively. The sheets are further connected into a network by means of C13–H13... $\pi$  (3.68 Å) contacts (Figure B5) The fingerprint plot of **pOHsaladpm** shows that the crystal packing is again ruled by H...H (51%) and C...H (34%)

intermolecular contacts, while the percentage of the O···H contacts (13%) in this compound is quite high (Figure 5b).

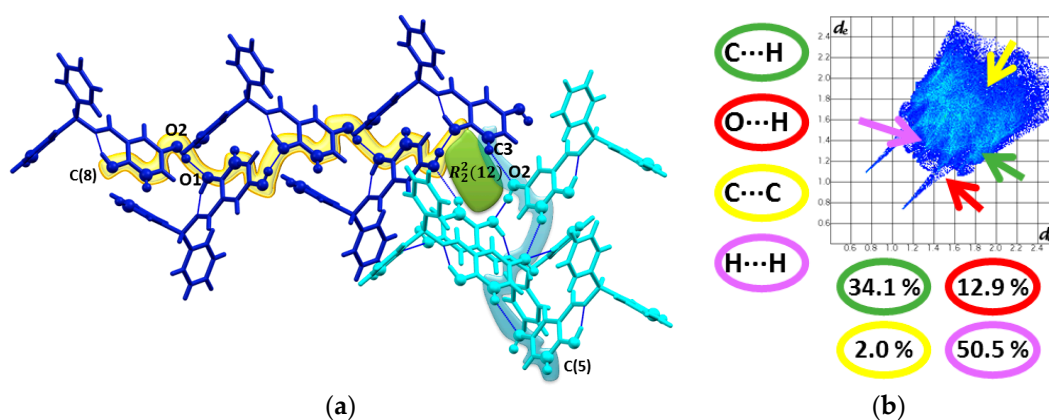


**Figure 5.** View of (a) chains of **pOHsaladpm** molecules formed by means of O–H···O and C–H···O interactions and (b) the 2D-fingerprint plot with marked corresponding regions: green arrow for C···H contacts, red arrows for O···H contacts, yellow arrow for C···C contacts and violet arrow for H···H contacts.

**mvnadpm** crystallizes in the  $P2_1/c$  space group of the monoclinic system with four molecules per unit cell, and the molecules are in enol-imine tautomeric form, while the O1 atom does not participate in intermolecular bonding. There is only one very weak interaction in the crystal structure of **mvnadpm**, namely C21–H21c···Cg(C1–C2–C3–C4–C5–C6), 3.508 Å. The fingerprint plot of **mvnadpm** shows that the crystal packing (Figure B6) is reigned by means of H···H (49%) and C···H (37%) intermolecular contacts (Figure 6b).

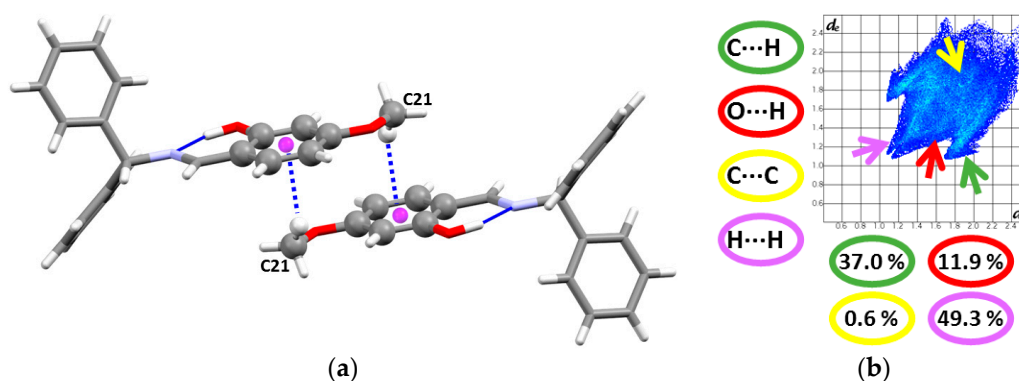


**Figure 6.** View of (a) a centrosymmetric dimer of **mvnadpm** molecules formed by means of C–H···Cg(C1 to C6) contacts and (b) the 2D-fingerprint plot with marked corresponding regions: green arrow for C···H contacts, red arrows for O···H contacts, yellow arrow for C···C contacts and violet arrow for H···H contacts.

### 2.3. NMR Study

Selected solid and solution state NMR study results of the investigated compounds are presented in Table 1, and all spectra are given in Appendix D, Figures D1–D12. One set of signals observed in  $^{13}\text{C}$  CP-MAS spectra of all investigated compounds (Figures D5–D12) and corresponding  $\delta\text{C2}$  values support the single-crystal X-ray diffraction results; enol-imine tautomeric form for **oOHsaladpm** ( $\delta\text{C2} = 152.37$  ppm), **pOHsaladpm** ( $\delta\text{C2} = 160.50$  ppm) and **mvnadpm** ( $\delta\text{C2} = 168.13$  ppm) and keto-amine tautomeric form for **mOHsaladpm** ( $\delta\text{C2} = 182.19$  ppm) in the solid state.

**Table 1.** Selected NMR chemical shifts (ppm) for investigated compounds in solid state and in CDCl<sub>3</sub> and DMSO-d<sub>6</sub> solutions, at 298 K. <sup>15</sup>N chemical shifts are reported relative to liquid ammonia.

Atom	State/Solvent	$\delta$ /ppm			
		oOHsaladpm	mOHsaladpm	pOHsaladpm	mvanadpm
OH	CDCl <sub>3</sub>	14.12	14.02	12.97	13.98
	DMSO	13.71	13.87	12.57	13.98
H7	CDCl <sub>3</sub>	8.39	8.34	8.35	8.34
	DMSO	8.75	9.90	8.71	8.67
C2	Solid	152.37	182.19	160.50	168.13
	CDCl <sub>3</sub>	150.96	164.18	155.06	164.03
	DMSO	150.03	163.45	153.35	163.66
C7	Solid	168.83	172.94	169.46	168.64
	CDCl <sub>3</sub>	164.86	164.04	164.51	164.10
	DMSO	166.71	165.52	165.89	165.55
N1	CDCl <sub>3</sub>	286.1	280.7	306.9	287.5
	DMSO	300.0	287.4	308.4	288.6

<sup>1</sup>H, <sup>13</sup>C and <sup>15</sup>N-NMR solution study indicated the presence of the enol-imine tautomeric form with the intramolecular O-H...N hydrogen bond in CDCl<sub>3</sub> and DMSO-d<sub>6</sub> solutions of all four investigated compounds; the measured  $\delta$ N1 values are in the range of 280.7–306.9 ppm in CDCl<sub>3</sub>, 288.6–308.4 in DMSO-d<sub>6</sub>, in addition to strongly deshielded proton OH signals in the range of 12.97–14.12 ppm in CDCl<sub>3</sub> and 12.57–13.98 in DMSO-d<sub>6</sub>.  $\delta$ C2 values of **oOHsaladpm**, **pOHsaladpm** and **mvanadpm** do not differ significantly in the solid state and in solution, supporting the same tautomeric form of those compounds in all investigated phases. On the other hand, the C2 signal of **mOHsaladpm** in CDCl<sub>3</sub> and DMSO-d<sub>6</sub> is observed at almost a 20-ppm lower value compared to the corresponding solid state signal, supporting the change of the keto-amine tautomeric form observed in the solid state. The lowest  $\delta$ N1 values in combination with the highest  $\delta$ OH values are observed for **mOHsaladpm** and **mvanadpm**, both in CDCl<sub>3</sub> and DMSO-d<sub>6</sub>, indicating a stronger intramolecular H-bond compared to the other two investigated compounds. This can be explained by the increased basicity of imine nitrogen atom due to electron donor effect of CH<sub>3</sub>O/OH substituents in *para*-position.

### 3. Materials and Methods

Powder X-ray diffraction (PXRD) experiments were performed on a PHILIPS PW 1840 X-ray diffractometer (Philips Analytical B. V., Almelo, The Netherlands) with CuK $\alpha$ 1 (1.54056 Å) radiation at 40 mA and 40 kV. The scattered intensities were measured with a scintillation counter. The angular range (2 $\theta$ ) was from 5–45° with steps of 0.02°, and the measuring time was 0.5 s per step. The data collection and analysis were performed using the program package Philips X'Pert [42–44].

Crystal and molecular structures were determined at 298 K using single crystal X-ray diffraction (SCXRD). Diffraction measurements were made on an Oxford Diffraction Xcalibur Kappa CCD X-ray diffractometer (Oxford Diffraction, Oxford, UK) with graphite-monochromated MoK $\alpha$  ( $\lambda$  = 0.71073 Å) radiation, and the instrument was operated using CrysAlis CCD and RED [45]. The datasets were collected using the  $\omega$  scan mode over the 2 $\theta$  range up to 54°. The structures were solved by direct methods and refined using the SHELXS and SHELXL programs, respectively [46]. The structural refinement was performed on  $F^2$  using all data. Hydrogen atoms not involved in hydrogen bonding were placed in calculated positions and treated as riding on their parent atoms (C–H = 0.93 Å and  $U_{\text{iso}}(\text{H}) = 1.2 U_{\text{eq}}(\text{C})$ ; C–H = 0.97 Å and  $U_{\text{iso}}(\text{H}) = 1.2 U_{\text{eq}}(\text{C})$ ), while the others were located from the electron difference map (Figure B2). All calculations were performed using the WinGX crystallographic suite of programs [47]. The data concerning the results of the crystallographic experiments are listed in Table B1. Further details are available from the Cambridge Crystallographic Centre (CCDC Deposition

Numbers 1509517, 1509518, 1509519 and 1509521). Molecular structures of compounds (Figure B1) and their packing diagrams (Figures B3–B6) were prepared using Mercury [48].

Solid state NMR spectra were recorded on Bruker Avance 300 spectrometer (Bruker, Rheinstetten, Germany) equipped with a 4-mm broad-band magic angle spinning (MAS) probe. The samples for  $^{13}\text{C}$  CP-MAS spectra were spun at the magic angle with 10 kHz. External references were adamantane and glycine. The spectra were acquired with 8000 scans and a repetition delay of 7 s.

1D ( $^1\text{H}$ ,  $^{13}\text{C}$ -DEPTq) and 2D (COSY, HSQC, HMBC,  $^1\text{H}$ - $^{15}\text{N}$ -HMBC) solution state NMR spectra were recorded on a Bruker Avance III HD 400 MHz/54 mm Ascend spectrometer (Bruker, Rheinstetten, Germany) equipped with a 5-mm PA BBI  $^1\text{H}/\text{D}$ -BB Z-GRAD probe head. All measurements were performed at 298 K using standard Bruker pulse programs.  $\text{CDCl}_3$  and  $\text{DMSO-d}_6$  were used as solvents and TMS as the internal standard for proton and carbon chemical shifts. Nitrogen chemical shifts were extracted from 2D  $^1\text{H}$ - $^{15}\text{N}$ -HMBC spectra and reported relative to liquid ammonia.

#### 4. Conclusions

Since the beginnings of the investigation of *o*-hydroxy Schiff base thermochromism, it was thought that imines with non-planar molecular geometry cannot show such phenomenon and that such molecules should be photochromic [1,2,4,18–21]. In the past decade, many non-planar *o*-hydroxy Schiff bases derived from benzylamine derivatives were synthesized and reported as thermochromic. There is still a general consensus that the deviation from the planarity, the dihedral angle between the aromatic subunits, can be up to  $25^\circ$  [25,26] for aniline derivatives, while *o*-hydroxy imines with a spacer between the imine N-atom and the aromatic rings of the corresponding amine are excluded from that empirical rule [27,28]. The accepted mechanism for thermochromism is a temperature-dependent keto-enol tautomeric change between an uncolored enol form and a yellow *cis*-keto form, while the existence of the *trans*-keto form changes the color to red [27,28]. In many cases, keto-amine forms were not found in the crystal structure *o*-hydroxy Schiff bases; in some cases, the molecules are in keto tautomeric form, and the samples are not of the expected color; and in some cases, keto-enol tautomeric equilibrium was found, and its position is affected by a temperature change without a color change; the postulates of Schiff base thermochromism are still taken as definite facts. The influence of the crystal packing is one of them. There are a few recent reports on photo- and thermo-chromism influenced by supramolecular interactions in crystals and co-crystals of *o*-hydroxy Schiff bases [5,7,10,11,27,30,32,49]. A rationalization of the intermolecular interactions has shown the influence of the molecular packing on the chromic properties and keto-enol tautomerism. Because of all that has been stated, the postulates of the Schiff base thermochromism should be thoroughly revised, while this work is one of those showing that imines derived from benzylamine derivatives can show thermochromism and that keto-enol tautomerism is under an impact of strong intermolecular interactions.

**Acknowledgments:** This research was supported by the University of Zagreb, Croatia, and the University of the Free State, South Africa.

**Author Contributions:** Marija Zbačnik and Katarina Pičuljan conceived and designed the experiments; Marija Zbačnik, Katarina Pičuljan and Jelena Parlov-Vuković performed the experiments; Marija Zbačnik and Katarina Pičuljan analyzed the data; Marija Zbačnik, Katarina Pičuljan, Jelena Parlov-Vuković, Predrag Novak and Andreas Roodt contributed reagents/materials/analysis tools; Marija Zbačnik, Katarina Pičuljan, Jelena Parlov-Vuković, Predrag Novak and Andreas Roodt wrote the paper.

**Conflicts of Interest:** The authors declare no conflict of interest. The founding sponsors had no role in the design of the study; in the collection, analyses or interpretation of data; in the writing of the manuscript; nor in the decision to publish the results.

#### Appendix A. Starting Materials, Systematic Names and Abbreviations

All reagents and solvents were purchased from commercial sources and used as received. Table A1 comprises all starting materials and solvents used for syntheses, crystallization or grinding experiments. Table A2 comprises systematic names of the obtained compounds.



**Table A1.** Starting materials used for various experiments.

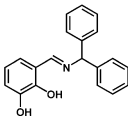
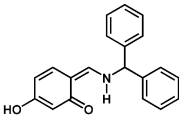
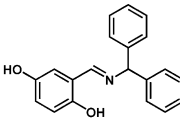
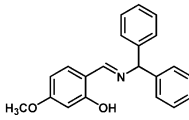
Name	Acronym	Manufacturer
2,3-dihydroxybenzaldehyde	oOH	Aldrich
2,4-dihydroxybenzaldehyde	mOH	Aldrich
2,5-dihydroxybenzaldehyde	pOH	Aldrich
<i>Meta</i> -vanillin	mvan	Aldrich
$\alpha$ -aminodiphenylmethane	adpm	Aldrich
Acetone	ace	CLARO-PROM
Chloroform	chl	Kemika
Ethanol	EtOH	Kemika

**Table A2.** Systematic names and acronyms of the compounds reported in this work.

Acronym	SYSTEMATIC NAME
oOHadpm	3-(Benzhydrylimino-methyl)-benzene-1,2-diol
mOHadpm	6-[(Benzhydryl-amino)-methylene]-3-hydroxy-cyclohexa-2,4-dienone
pOHadpm	2-(Benzhydrylimino-methyl)-benzene-1,4-diol
mvanadpm	2-(Benzhydrylimino-methyl)-5-methoxy-phenol

## Appendix B. Crystallographic Study

**Table B1.** General and crystallographic data for compounds reported in this work.

Acronym	oOHsaladpm	mOHsaladpm	pOHsaladpm	mvanadpm
Structural formula				
Molecular formula	C <sub>20</sub> H <sub>17</sub> NO <sub>2</sub>	C <sub>20</sub> H <sub>17</sub> NO <sub>2</sub>	C <sub>20</sub> H <sub>17</sub> NO <sub>2</sub>	C <sub>21</sub> H <sub>19</sub> NO <sub>2</sub>
<i>M<sub>r</sub></i>	303.35	303.35	303.35	317.37
Crystal system	Triclinic		Monoclinic	
Space group	<i>P</i> $\bar{1}$		<i>P</i> 2 <sub>1</sub> / <i>c</i>	
<i>a</i> /Å	5.9123(4)	13.7525(7)	13.7483(10)	17.1517(5)
<i>b</i> /Å	11.2287(7)	9.8109(4)	10.8460(5)	6.0402(2)
<i>c</i> /Å	12.0481(7)	17.6387(9)	11.5168(8)	16.5078(5)
$\alpha$ /°	92.719(5)		90	
$\beta$ /°	91.521(5)	138.286(3)	113.745(8)	93.783(3)
$\gamma$ /°	91.338(5)		90	
<i>V</i> /Å <sup>3</sup>	798.42(9)	1583.61(15)	1571.9(2)	1706.48(9)
<i>Z</i>	2		4	
<i>D</i> <sub>calc</sub> /g·cm <sup>−3</sup>	1.262	1.272	1.282	1.235
$\lambda$ (MoK $\alpha$ )/Å	0.71073			
$\mu$ /mm <sup>−1</sup>	0.081	0.082	0.083	0.079
Crystal size/mm	0.91 × 0.25 × 0.24	0.81 × 0.19 × 0.06	0.91 × 0.37 × 0.08	0.67 × 0.44 × 0.25
<i>F</i> (000)	320	640	640	672
Refl. collected/unique	8332/3459	6195/2738	9983/3398	10,616/2984
No. of restraints	0	0	1	0
Parameters	216	216	216	223
<i>R</i> [ <i>F</i> <sup>2</sup> ≥ 2 $\sigma$ ( <i>F</i> <sup>2</sup> )]	0.0375	0.0342	0.0393	0.0324
<i>wR</i> ( <i>F</i> <sup>2</sup> )	0.0982	0.0670	0.0916	0.0918
Goodness-of-fit, <i>S</i>	0.842	0.816	0.823	0.916
CCDC deposition number	1509517	1509518	1509519	1509521

**Table B2.** Values of C2–O1 and C7–N1 bond distances and of dihedral angles (dihedral angle: the angle between best planes calculated trough:  $\phi_1$ , C1–C6 and C9–C14 rings;  $\phi_2$ , C1–C6 and C15–C20 rings).

Compound	$d(\text{C2–O1})/\text{\AA}$	$d(\text{C7–N1})/\text{\AA}$	$\phi_1/^\circ$	$\phi_2/^\circ$
oOHsaladpm	1.352(2)	1.274(2)	65.30(4)	70.69(4)
mOHsaladpm	1.298(0)	1.305(0)	88.76(0)	78.54(0)
pOHsaladpm	1.362(1)	1.280(1)	89.95(0)	76.71(0)
mvanadpm	1.348(2)	1.276(2)	45.02(4)	72.65(4)

**Table B3.** Hydrogen bond geometry ( $\text{\AA}$ ,  $^\circ$ ) in compound oOHsaladpm. *D*, donor atom; *A*, acceptor atom.

D–H...A	$d(\text{D...A})/\text{\AA}$	$\angle(\text{D–H...A})/^\circ$	Symmetry Operator
O1–H1...N1 *	2.562(1)	152(2)	$x, y, z$
O2–H2...O1	2.794(1)	150(2)	$-x, -y + 2, -z + 1$
C10–H10...O2	3.533(2)	135(0)	$-x, -y + 2, -z + 1$

\* Intramolecular.

**Table B4.** Hydrogen bond geometry ( $\text{\AA}$ ,  $^\circ$ ) in compound mOHsaladpm.

D–H...A	$d(\text{D...A})/\text{\AA}$	$\angle(\text{D–H...A})/^\circ$	Symmetry Operator
N1–H1...O1 *	2.594(0)	141.34(0)	$x, y, z$
O2–H2...O1	2.572(0)	172.49(0)	$-x, y + 1/2, -z + 1/2 + 1$
C18–H18...O1	3.504(0)	155.82(0)	$-x + 1, -y + 1, -z + 1$
C11–H11...O1	3.534(0)	166.18(0)	$-x, y - 1, z + 2$
C3–H3...O1	2.691(0)	121.56(0)	$-x, y + 1/2, -z + 1/2 + 1$
C8–H8...O2	3.397(0)	177.69(0)	$x, y - 1, z$

\* Intramolecular.

**Table B5.** Hydrogen bond geometry ( $\text{\AA}$ ,  $^\circ$ ) in compound pOHsaladpm.

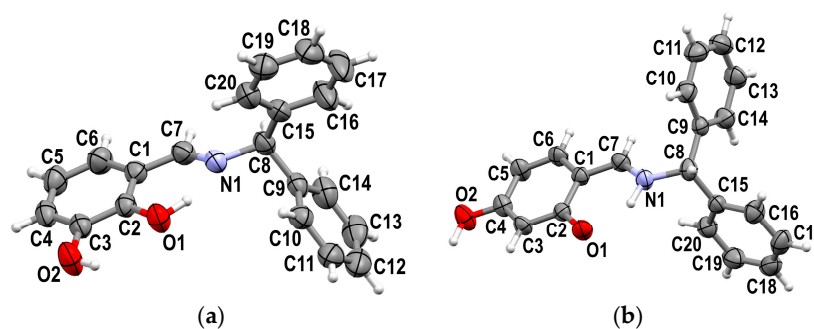
D–H...A	$d(\text{D...A})/\text{\AA}$	$\angle(\text{D–H...A})/^\circ$	Symmetry Operator
O1–H1...N1 *	2.539(0)	149.97(0)	$x, y, z$
O2–H2...O1	2.801(0)	166.19(0)	$-x, y + 1/2, -z + 1/2$
C3–H3...O2	3.456(0)	138.80(0)	$x, -y + 1/2 + 1, z - 1/2$

\* Intramolecular.

**Table B6.** Hydrogen bond geometry ( $\text{\AA}$ ,  $^\circ$ ) in compound mvanadpm.

D–H...A	$d(\text{D...A})/\text{\AA}$	$\angle(\text{D–H...A})/^\circ$	Symmetry Operator
O1–H1...N1 *	2.613(1)	148(2)	$x, y, z$

\* Intramolecular.

**Figure B1.** Cont.

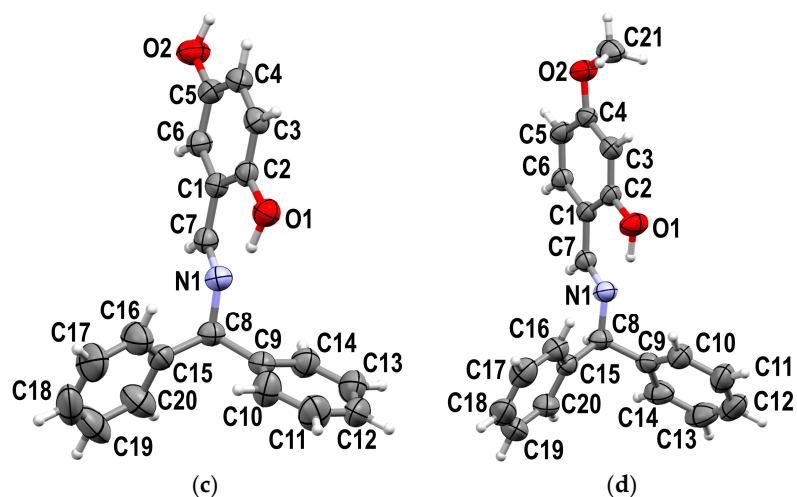


**Figure B1.** Thermal ellipsoids (50%) plots of (a) oOHsaladpm, (b) mOHsaladpm, (c) pOHsaladpm and (d) mvnadp showing atom-labelling schemes. H atoms are shown as small spheres of arbitrary radius.

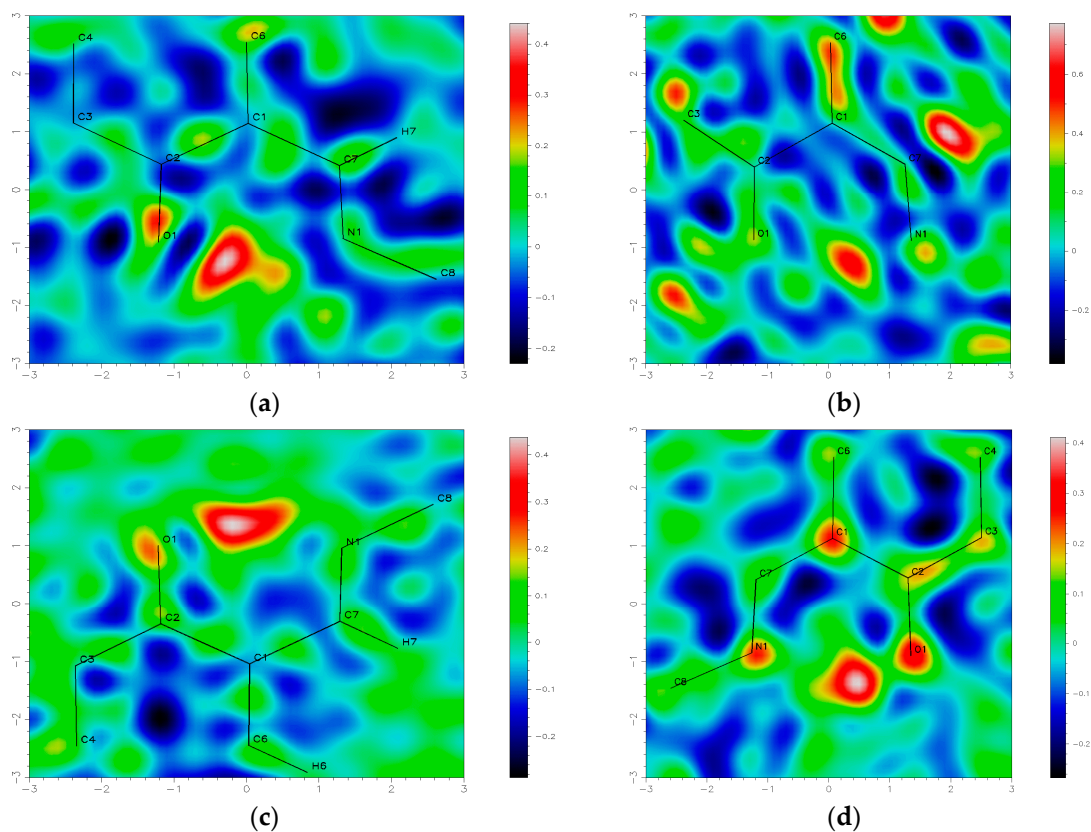


**Figure B2.** Contour  $\delta F$  maps calculated through N1–C7–C1–C2–O1 chelate rings of (a) oOHsaladpm, (b) mOHsaladpm, (c) pOHsaladpm and (d) mvnadp with pronounced maximum representing the residual electron density corresponding to the position of the H1 atom in the intramolecular H-bond.

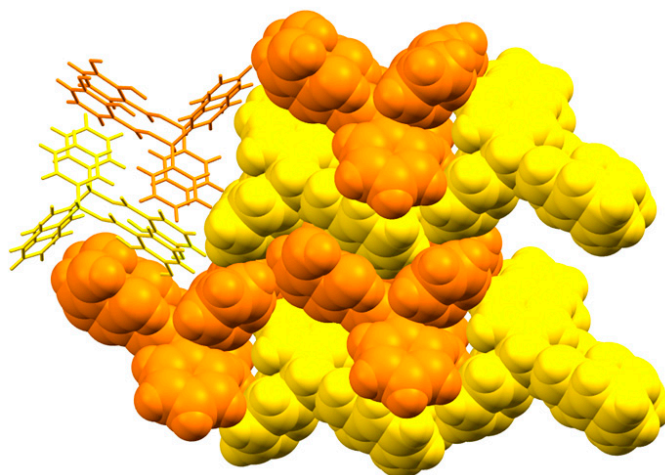


Figure B3. Packing diagram for oOHsaladpm.

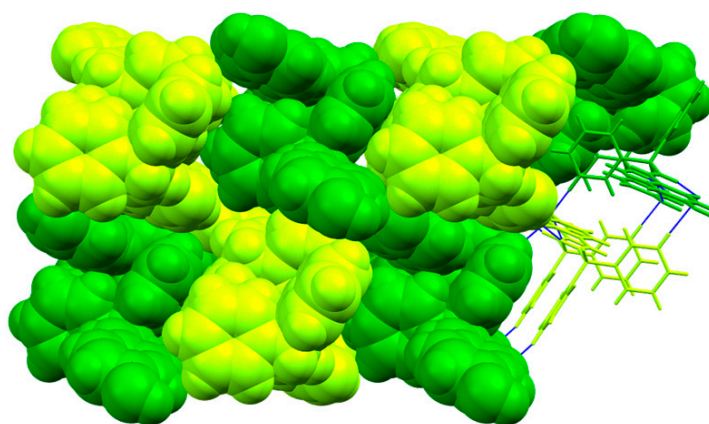


Figure B4. Packing diagram for mOHsaladpm.

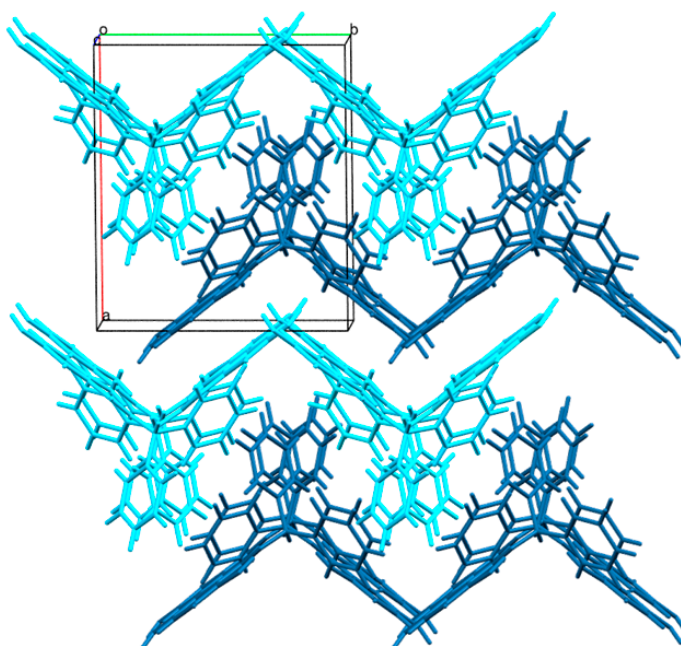


Figure B5. Packing diagram for pOHsaladpm.

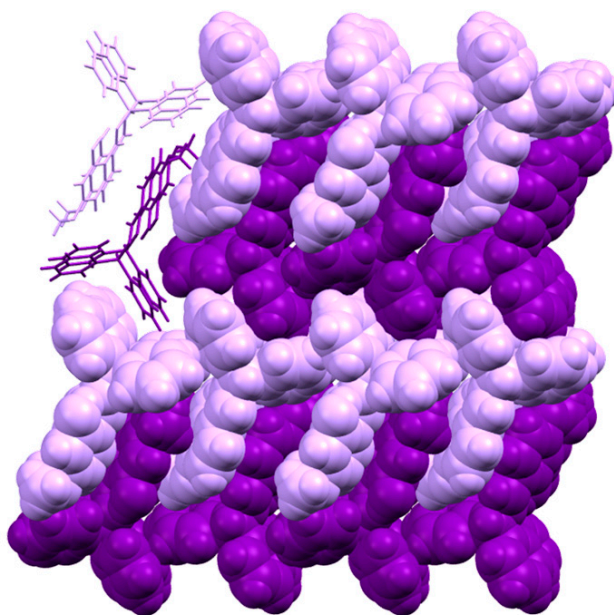


Figure B6. Packing diagram for **mvanadpm**.

### Appendix C. Thermal Study

DSC measurements were performed on a Mettler Toledo DSC823<sup>e</sup> module and TG experiments on a **Mettler Toledo TGA/SDTA 851** thermobalance in sealed aluminum pans (40  $\mu$ L), heated in flowing nitrogen (200 mL·min<sup>−1</sup>) at a rate of 10 °C·min<sup>−1</sup>. The data collection and analysis was performed using the program package STARe Software 14.00 [45].

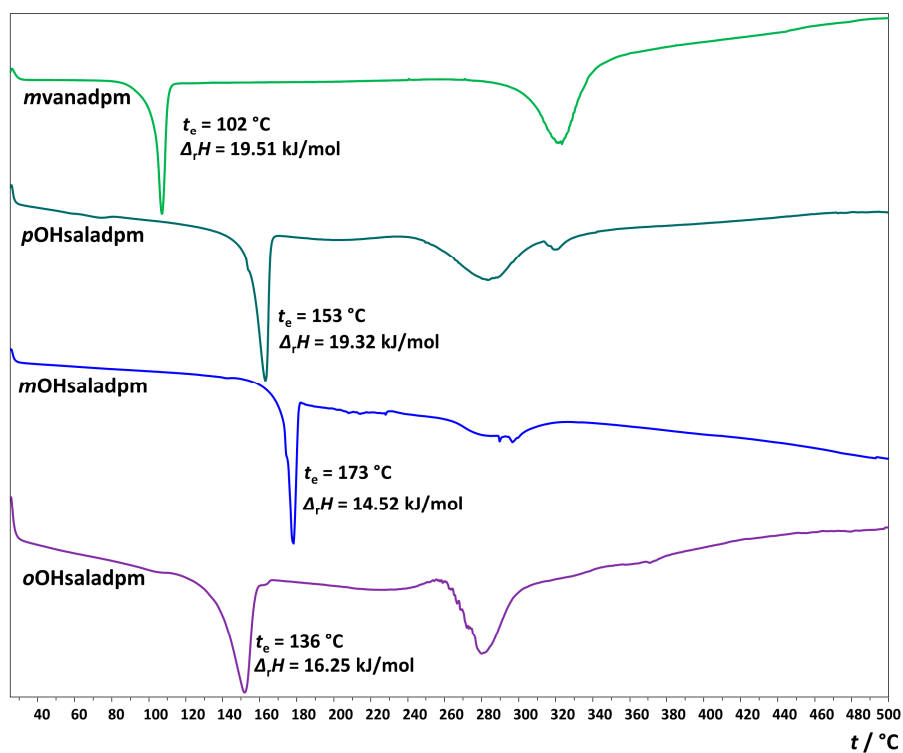


Figure C1. DSC curves of **oOHsaladpm** (purple), **mOHsaladpm** (blue), **pOHsaladpm** (turquoise) and **mvanadpm** (green).



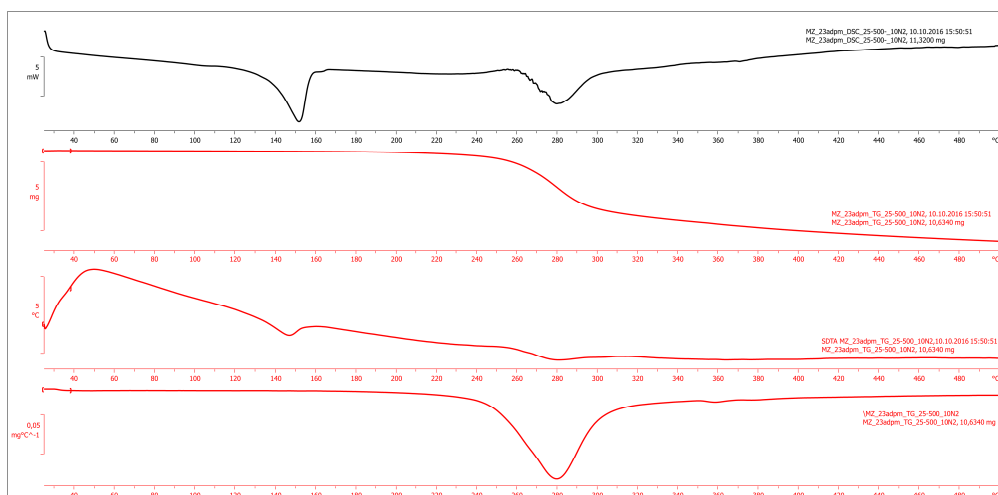


Figure C2. DSC, TG, SDTA and DTG curves of oOHsaladpm.

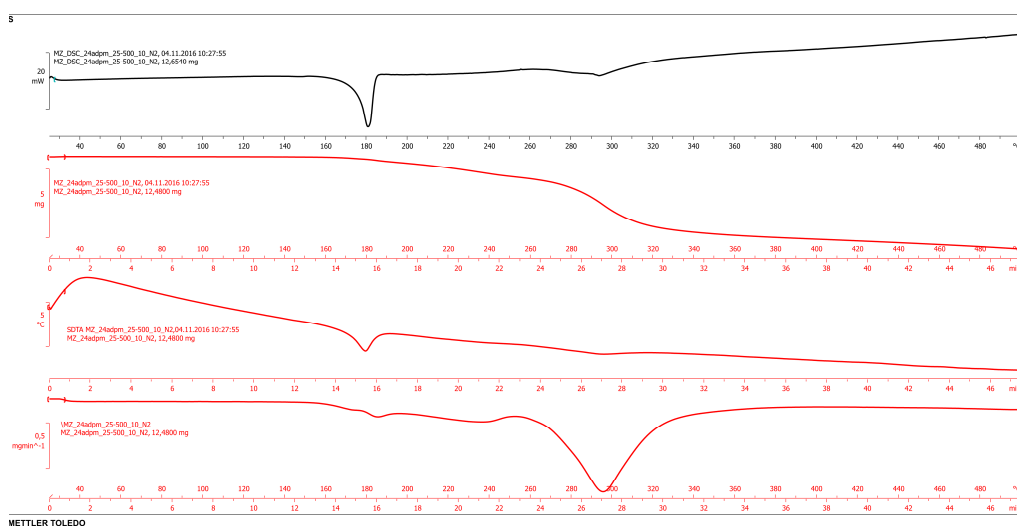


Figure C3. DSC, TG, SDTA and DTG curves of mOHsaladpm.

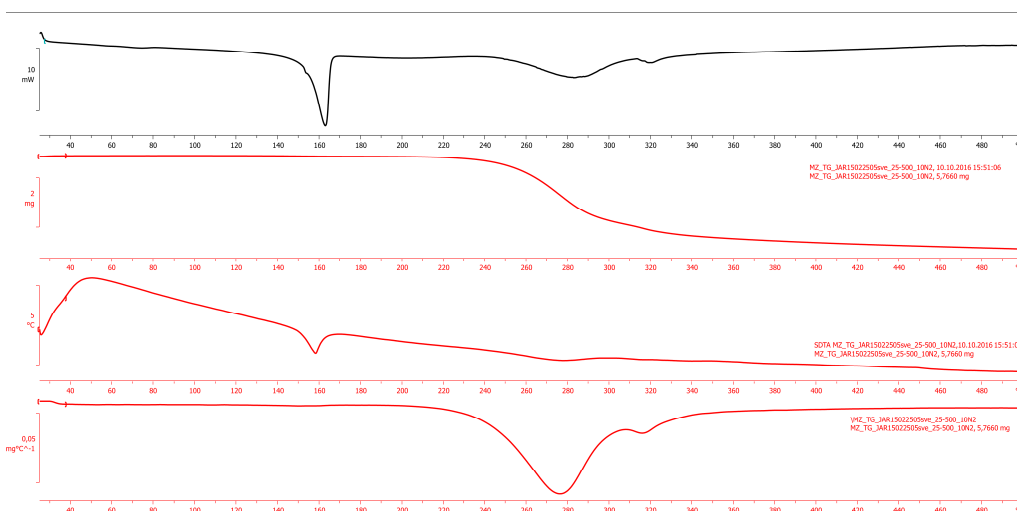


Figure C4. DSC, TG, SDTA and DTG curves of pOHsaladpm.

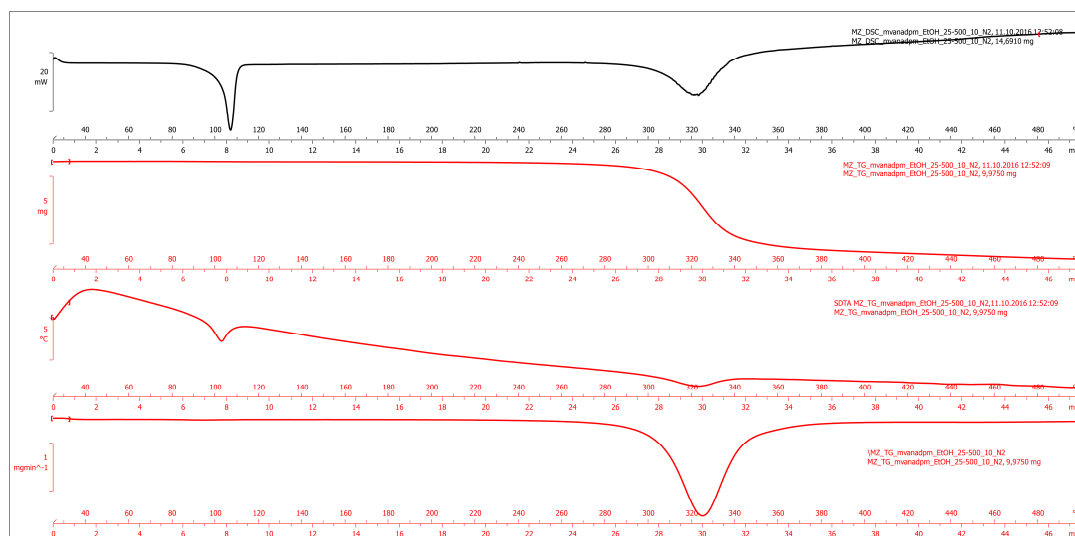


Figure C5. DSC, TG, SDTA and DTG curves of *mvanadpm*.

## Appendix D. NMR Study

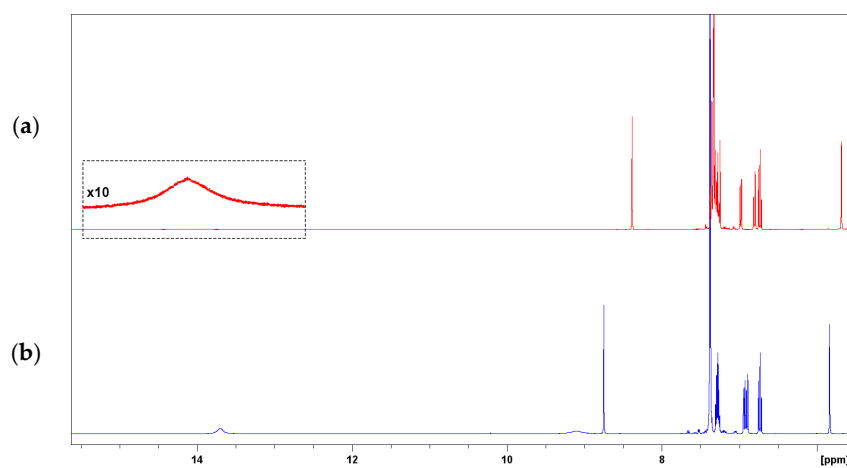


Figure D1.  $^1\text{H}$ -NMR spectra of *oOHsaladpm* in (a)  $\text{CDCl}_3$  and (b)  $\text{DMSO-d}_6$ .

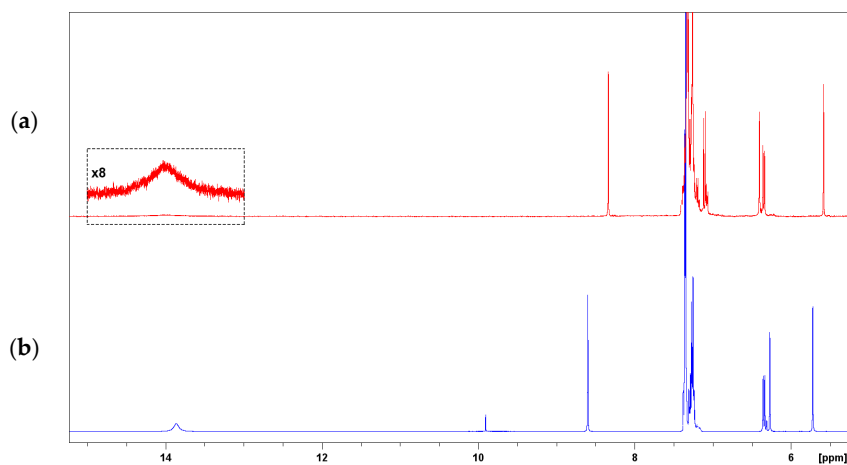
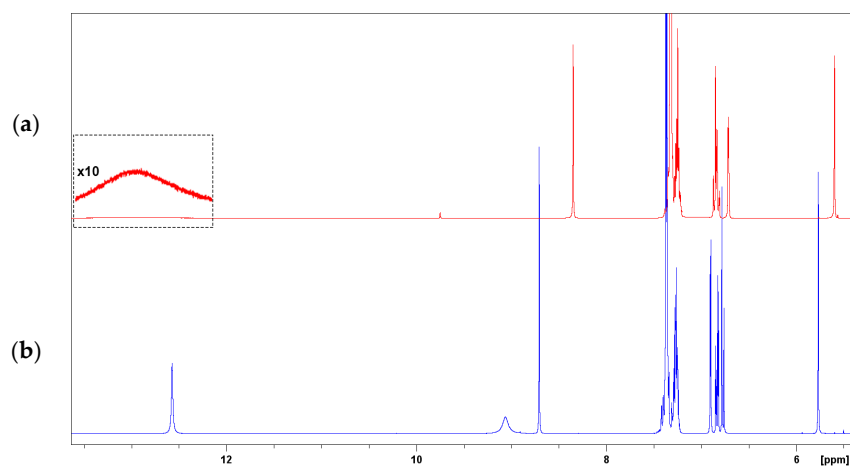
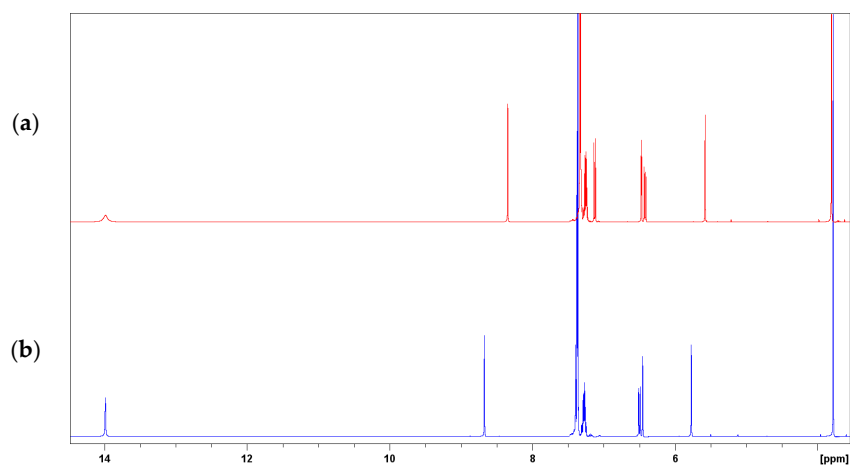


Figure D2.  $^1\text{H}$ -NMR spectra of *mOHsaladpm* in (a)  $\text{CDCl}_3$  and (b)  $\text{DMSO-d}_6$ .



**Figure D3.**  $^1\text{H}$ -NMR spectra of **pOHsaladpm** in (a)  $\text{CDCl}_3$  and (b)  $\text{DMSO-d}_6$ .



**Figure D4.**  $^1\text{H}$ -NMR spectra of **mvnadpm** in (a)  $\text{CDCl}_3$  and (b)  $\text{DMSO-d}_6$ .

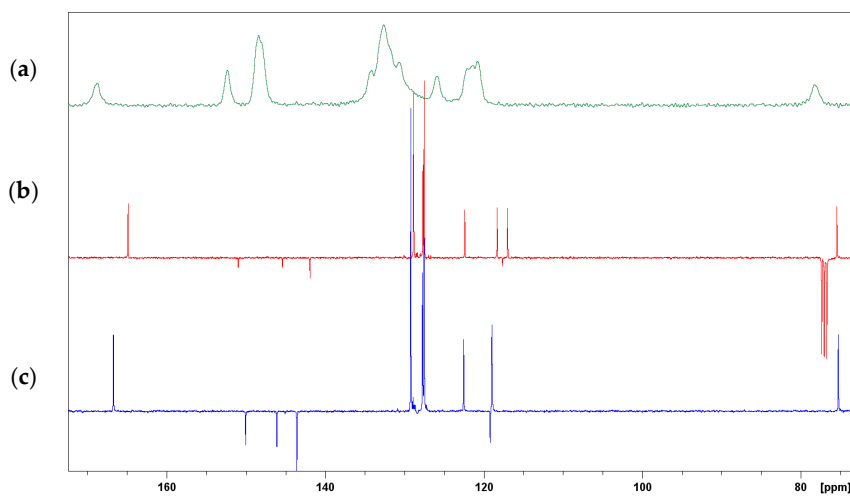


**Figure D5.** A comparison of solid state  $^{13}\text{C}$  CP-MAS spectrum of **oOHsaladpm** (a) with solution state  $^{13}\text{C}$ -DEPTq spectra in  $\text{CDCl}_3$  (b) and  $\text{DMSO-d}_6$  (c).

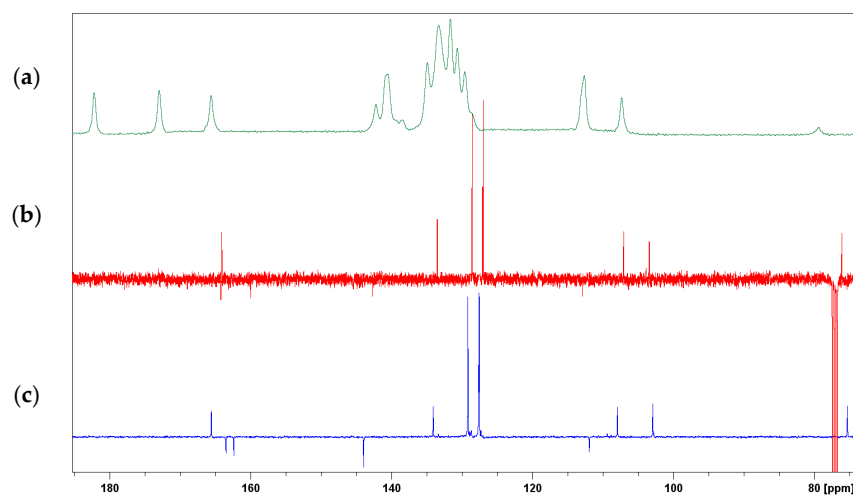


**Figure D6.** A comparison of solid state  $^{13}\text{C}$  CP-MAS spectrum of **mOHsaladpm** (a) with solution state  $^{13}\text{C}$ -DEPTq spectra in  $\text{CDCl}_3$  (b) and  $\text{DMSO-d}_6$  (c).

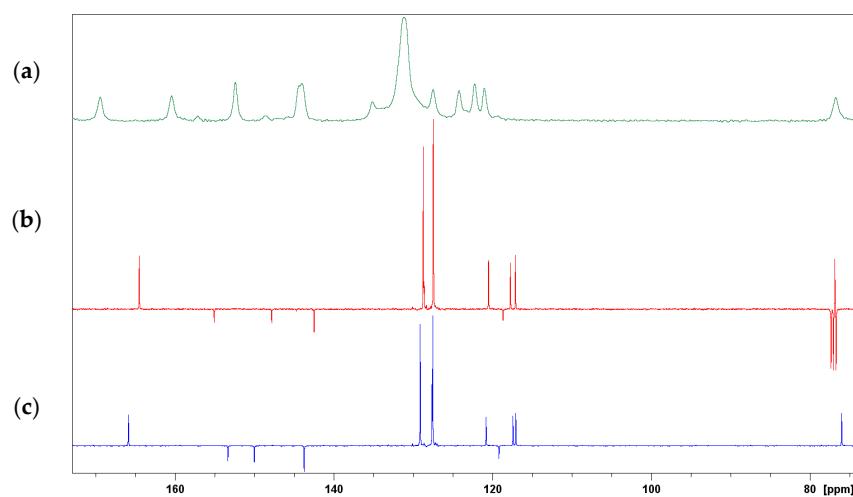


**Figure D7.** A comparison of solid state  $^{13}\text{C}$  CP-MAS spectrum of **pOHsaladpm** (a) with solution state  $^{13}\text{C}$ -DEPTq spectra in  $\text{CDCl}_3$  (b) and  $\text{DMSO-d}_6$  (c).

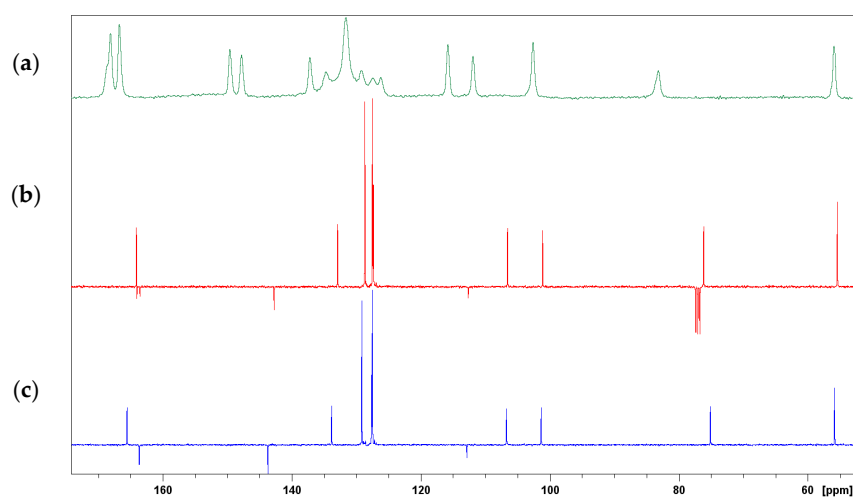


**Figure D8.** A comparison of solid state  $^{13}\text{C}$  CP-MAS spectrum of **mvnadpm** (a) with solution state  $^{13}\text{C}$ -DEPTq spectra in  $\text{CDCl}_3$  (b) and  $\text{DMSO-d}_6$  (c).

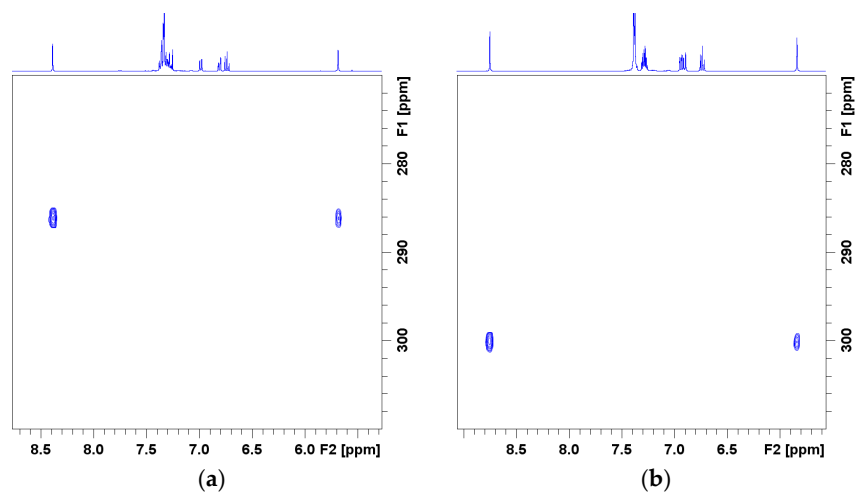


Figure D9.  $^1\text{H}$ - $^{15}\text{N}$  HMBC NMR spectra of **oOHsaladpm** in (a)  $\text{CDCl}_3$  and (b)  $\text{DMSO-d}_6$ .

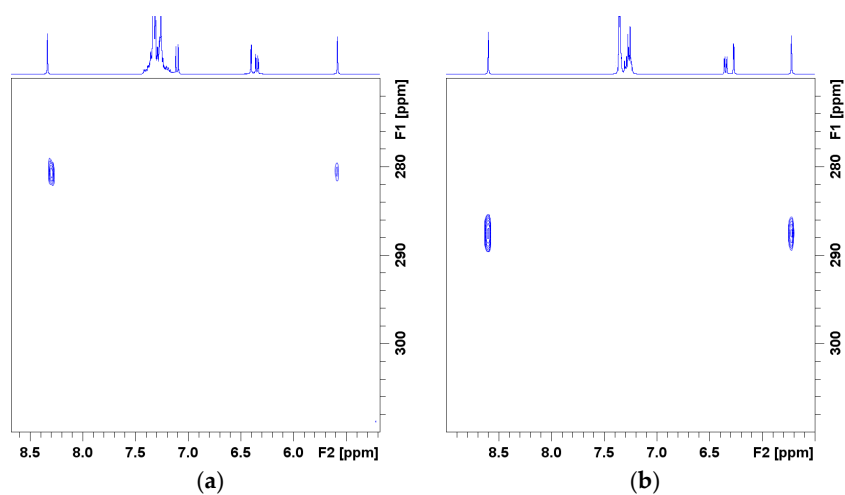


Figure D10.  $^1\text{H}$ - $^{15}\text{N}$  HMBC NMR spectra of **mOHsaladpm** in (a)  $\text{CDCl}_3$  and (b)  $\text{DMSO-d}_6$ .

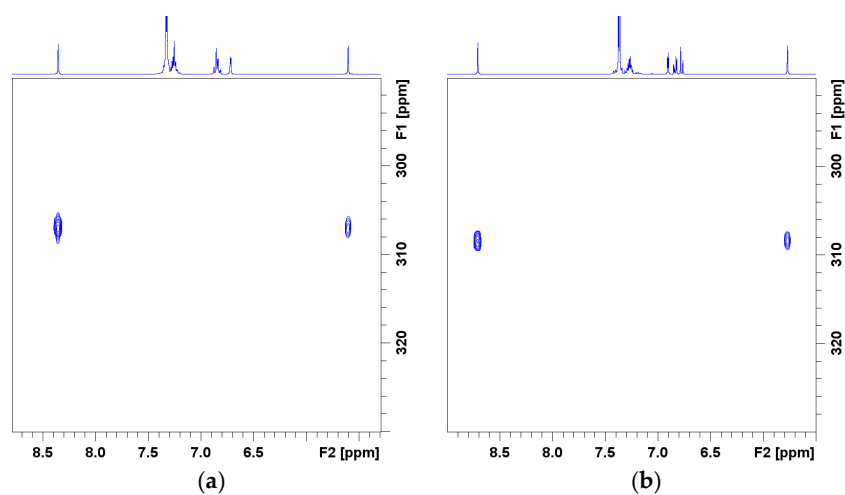


Figure D11.  $^1\text{H}$ - $^{15}\text{N}$  HMBC NMR spectra of **pOHsaladpm** in (a)  $\text{CDCl}_3$  and (b)  $\text{DMSO-d}_6$ .



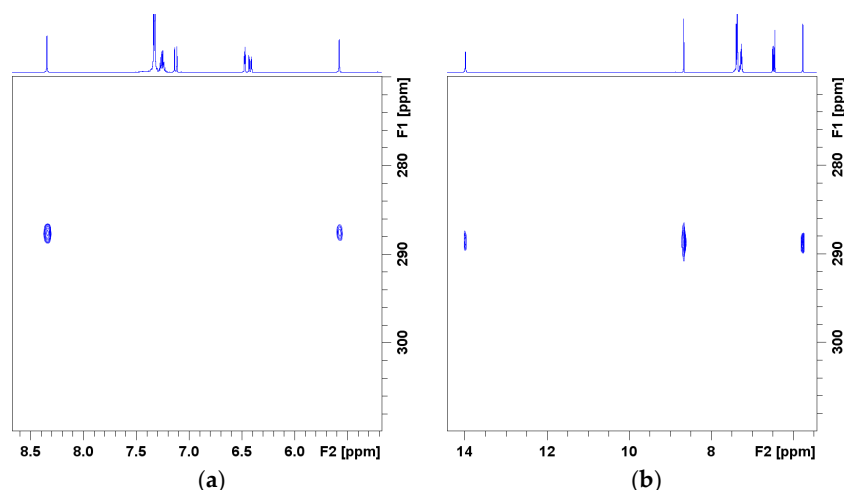


Figure D12.  $^1\text{H}$ - $^{15}\text{N}$  HMBC NMR spectra of **mvanadpm** in (a)  $\text{CDCl}_3$  and (b)  $\text{DMSO-d}_6$ .

## References

1. Bouas-Laurent, H.; Dürr, H. Organic Photochromism. *Pure Appl. Chem.* **2001**, *73*, 639–665. [[CrossRef](#)]
2. Grubb, W.T.; Kistiakowsky, G.B. On the Nature of Thermochromism. *J. Am. Chem. Soc.* **1950**, *72*, 419–424. [[CrossRef](#)]
3. Day, J.H. Thermochromism of inorganic compounds. *Chem. Rev.* **1968**, *68*, 649–657. [[CrossRef](#)]
4. Day, J.H. Thermochromism. *Chem. Rev.* **1963**, *63*, 65–80. [[CrossRef](#)]
5. Carletta, A.; Buol, X.; Leyssens, T.; Champagne, B.; Wouters, J. Polymorphic and Isomorphic Cocrystals of a *N*-Salicylidene-3-aminopyridine with Dicarboxylic Acids: Tuning of Solid-State Photo- and Thermochromism. *J. Phys. Chem. C* **2016**, *120*, 10001–10008. [[CrossRef](#)]
6. Staehle, I.O.; Rodríguez-Molina, B.; Khan, S.I.; Garcia-Garibay, M.A. Engineered Photochromism in Crystalline Salicylidene Anilines by Facilitating Rotation to Reach the Colored *trans*-Keto Form. *Cryst. Growth Des.* **2014**, *14*, 3667–3673. [[CrossRef](#)]
7. Johmoto, K.; Sekine, A.; Uekusa, H. Photochromism Control of Salicylideneaniline Derivatives by Acid–Base Co-Crystallization. *Cryst. Growth Des.* **2012**, *12*, 4779–4786. [[CrossRef](#)]
8. Robert, F.; Naik, A.D.; Hidara, F.; Tinant, B.; Robiette, R.; Wouters, J.; Garcia, Y. Engineering Solid-State Molecular Switches: *N*-Salicylidene *N*-Heterocycle Derivatives. *Eur. J. Org. Chem.* **2010**, 621–637. [[CrossRef](#)]
9. Naik, A.D.; Fontaine, G.; Bellayer, S.; Bourbigot, S. Salen based Schiff bases to flame retard thermoplastic polyurethane mimicking operational strategies of thermosetting resin. *RSC Adv.* **2015**, *5*, 48224–48235. [[CrossRef](#)]
10. Zbačnik, M.; Vitković, M.; Vulić, V.; Nogalo, I.; Cinčić, D. Competition between Halogen Bonds in Cocrystals of Imines Derived from *o*-Vanillin. *Cryst. Growth Des.* **2016**, *16*, 6381–6389. [[CrossRef](#)]
11. Mercier, G.M.; Robeyns, K.; Leyssens, T. Altering the Photochromic Properties of *N*-Salicylideneanilines Using a Co-Crystal Engineering Approach. *Cryst. Growth Des.* **2016**, *16*, 3198–3205. [[CrossRef](#)]
12. Schiff, H. Mittheilungen aus dem Universitätslaboratorium in Pisa: Eine neue Reihe organischer Basen. *Justus Liebigs Ann. Chim.* **1864**, *131*, 118–119. [[CrossRef](#)]
13. Proetto, M.; Liu, W.; Hagenbach, A.; Abram, U.; Gust, R. Synthesis, characterization and in vitro antitumour activity of a series of novel platinum(II) complexes bearing Schiff base ligands. *Eur. J. Med. Chem.* **2012**, *53*, 168. [[CrossRef](#)] [[PubMed](#)]
14. Vicini, P.; Geronikaki, A.; Incerti, M.; Busonera, B.; Poni, G.; Cabras, C.A.; Colla, P.L. Synthesis and biological evaluation of benzo[d]isothiazole, benzothiazole and thiazole Schiff bases. *Bioorg. Med. Chem.* **2003**, *11*, 4785–4789. [[CrossRef](#)]
15. Khan, K.M.; Rahim, F.; Ambreen, N.; Taha, M.; Khan, M.; Jahan, H.; Najeebullah, U.; Shaikh, A.; Iqbal, S.; Perveen, S.; et al. Synthesis of benzophenonehydrazone Schiff bases and their in vitro antiglycating activities. *Med. Chem.* **2013**, *9*, 588–595. [[CrossRef](#)] [[PubMed](#)]

16. De Lucas Chazin, E.; de Souza Sanches, P.; Lindgren, E.B.; Vellasco Júnior, W.T.; Pinto, L.C.; Rodríguez Burbano, R.M.; Yoneda, J.D.; Zaccur Leal, K.; Brandão Gomes, C.R.; Wardell, J.L.; et al. Synthesis and Biological Evaluation of Novel 6-Hydroxy-benzo[d][1,3]oxathiol-2-one Schiff Bases as Potential Anticancer Agents. *Molecules* **2015**, *20*, 1968–1983. [[CrossRef](#)] [[PubMed](#)]
17. Blagus, A.; Cinčić, D.; Friščić, T.; Kaitner, B.; Stilinović, V. Schiff bases derived from hydroxyaryl aldehydes: molecular and crystal structure, tautomerism, quinoid effect, coordination compounds. *Maced. J. Chem. Chem. Eng.* **2010**, *29*, 117–138.
18. Cohen, M.D.; Schmidt, G.M.J. Photochromy and thermochromy of anils. *J. Phys. Chem.* **1962**, *66*, 2442–2446. [[CrossRef](#)]
19. Cohen, M.D.; Schmidt, G.M.J.; Flavian, S. Topochemistry. Part VI. Experiments on photochromy and thermochromy of crystalline anils of salicylaldehydes. *J. Chem. Soc.* **1964**, 2041–2051. [[CrossRef](#)]
20. Cohen, M.D.; Hirshberg, Y.; Schmidt, G.M.J. Topochemistry. Part VII. The photoactivity of anils of salicylaldehydes in rigid solutions. *J. Chem. Soc.* **1964**, 2051–2059. [[CrossRef](#)]
21. Bergman, J.; Leiserowitz, L.; Schmidt, G.M.J. Topochemistry. Part IX. The crystal and molecular structures of *N*-5-chlorosalicylideneaniline near 90 and 300°K. *J. Chem. Soc.* **1964**, 2068–2085. [[CrossRef](#)]
22. Hadjoudis, E.; Vittorakis, M.; Mavridis, I.M. Photochromism and thermochromism of Schiff bases in the solid state and in rigid glasses. *Tetrahedron* **1987**, *43*, 1345–1360. [[CrossRef](#)]
23. Ogawa, K.; Kasahara, Y.; Ohtani, Y.; Harada, J. Crystal Structure Change for the Thermochromy of *N*-Salicylideneanilines. The First Observation by X-ray Diffraction. *J. Am. Chem. Soc.* **1998**, *120*, 7107–7108. [[CrossRef](#)]
24. Harada, J.; Fujiwara, T.; Ogawa, K. Crucial Role of Fluorescence in the Solid-State Thermochromism of Salicylideneanilines. *J. Am. Chem. Soc.* **2007**, *129*, 16216–16221. [[CrossRef](#)] [[PubMed](#)]
25. Hadjoudis, E.; Rontoyianni, A.; Ambroziak, K.; Dziembowska, T.; Mavridis, I.M. Photochromism and thermochromism of solid *trans*-*N,N'*-bis-(salicylidene)-1,2-cyclohexanediamines and *trans*-*N,N'*-bis-(2-hydroxy-naphylidene)-1,2-cyclohexanediamine. *J. Photochem. Photobiol. A* **2004**, *162*, 521–530. [[CrossRef](#)]
26. Hadjoudis, E.; Mavridis, I.M. Photochromism and thermochromism of Schiff bases in the solid state: structural aspects. *Chem. Soc. Rev.* **2004**, *33*, 579–588. [[CrossRef](#)] [[PubMed](#)]
27. Robert, F.; Naik, A.D.; Tinant, B.; Robiette, R.; Garcia, Y. Insights into the Origin of Solid-State Photochromism and Thermochromism of *N*-Salicylideneanils: The Intriguing Case of Aminopyridines. *Chem. A Eur. J.* **2009**, *15*, 4327–4342. [[CrossRef](#)] [[PubMed](#)]
28. Robert, F.; Jacquemin, P.-L.; Tinant, B.; Garcia, Y. *Trans*-keto\* form detection in non-photochromic *N*-salicylidene aminomethylpyridines. *CrystEngComm* **2012**, *14*, 4396–4406. [[CrossRef](#)]
29. Kaitner, B.; Zbačnik, M. Solvent-free Mechanochemistry of Two Thermochromic Schiff Bases. *Acta Chim. Slov.* **2012**, *59*, 670–679. [[PubMed](#)]
30. Zbačnik, M.; Kaitner, B. Ex situ and in situ monitoring of the syntheses of thermochromic Schiff bases. *CrystEngComm* **2014**, *16*, 4162–4168. [[CrossRef](#)]
31. Zbačnik, M.; Nogalo, I.; Cinčić, D.; Kaitner, B. Polymorphism control in the mechanochemical and solution-based synthesis of a thermochromic Schiff base. *CrystEngComm* **2015**, *17*, 7870–7877. [[CrossRef](#)]
32. Zbačnik, M.; Kaitner, B. Supramolecular Influence on Keto-Enol Tautomerism and Thermochromic Properties of *o*-Hydroxy Schiff Bases. *Croat. Chem. Acta* **2016**, *89*, 125–132. [[CrossRef](#)]
33. James, S.L.; Adams, C.J.; Bolm, C.; Braga, D.; Collier, P.; Friščić, T.; Grepioni, F.; Harris, K.D.M.; Hyett, G.; Jones, W.; et al. Mechanochemistry: Opportunities for new and cleaner synthesis. *Chem. Soc. Rev.* **2012**, *41*, 413–447. [[CrossRef](#)] [[PubMed](#)]
34. Cinčić, D.; Brekalo, I.; Kaitner, B. Effect of atmosphere on solid-state amine-aldehyde condensations: Gas-phase catalysts for solid-state transformations. *Chem. Commun.* **2012**, *48*, 11683–11685. [[CrossRef](#)] [[PubMed](#)]
35. Tanaka, K.; Toda, F. Solvent-Free Organic Synthesis. *Chem. Rev.* **2000**, *100*, 1025–1074. [[CrossRef](#)] [[PubMed](#)]
36. Carletta, A.; Dubois, J.; Tilborg, A.; Wouters, J. Solid-state investigation on a new dimorphic substituted *N*-salicylidene compound: Insights into its thermochromic behavior. *CrystEngComm* **2015**, *17*, 3509–3518. [[CrossRef](#)]
37. Hansen, P.E.; Rozwadowski, Z.; Dziembowska, T. NMR Studies of Hydroxy Schiff Bases. *Curr. Org. Chem.* **2009**, *13*, 194–215. [[CrossRef](#)]

38. Claramunt, R.M.; López, C.; Santa María, M.D.; Sanz, D.; Elguero, J. The use of NMR spectroscopy to study tautomerism. *Prog. Nucl. Magn. Reson. Spectrosc.* **2006**, *49*, 169–206. [[CrossRef](#)]
39. Novak, P.; Jednačak, T.; Parlov Vuković, J.; Zangger, K.; Rubčić, M.; Galić, N.; Hrenar, T. Synthesis, structural characterization and hydrogen bonding of mono(salicylidene)carbohydrazide. *Croat. Chem. Acta* **2012**, *85*, 451–456. [[CrossRef](#)]
40. Rubčić, M.; Galić, N.; Halasz, I.; Jednačak, T.; Judaš, N.; Plavec, J.; Šket, P.; Novak, P. Multiple solid forms of 1,5-bis(salicylidene)carbohydrazide: Polymorph-modulated thermal reactivity. *Cryst. Growth Des.* **2014**, *14*, 2900–2912. [[CrossRef](#)]
41. Novak, P.; Pičuljan, K.; Hrenar, T.; Biljan, T.; Meić, Z. Hydrogen bonding and solution state structure of Salicylaldehyde-4-phenylthiosemicarbazone. A Combined Experimental and Theoretical Study. *J. Mol. Struct.* **2009**, *919*, 66–71. [[CrossRef](#)]
42. *Philips X'Pert Data Collector 1.3e*; Philips Analytical B. V.: Almelo, Netherlands, 2001.
43. *Philips X'Pert Graphic & Identify 1.3e*; Philips Analytical B. V.: Almelo, Netherlands, 2001.
44. *Philips X'Pert Plus 1.0*; Philips Analytical B. V.: Almelo, Netherlands, 1999.
45. Oxford Diffraction. *CrysAlis CCD and CrysAlis RED*; Version 1.170.; Oxford Diffraction Ltd.: Wroclaw, Poland, 2003.
46. Sheldrick, G.M. A short history of SHELX. *Acta Crystallogr.* **2008**, *A64*, 112–122. [[CrossRef](#)] [[PubMed](#)]
47. Macrae, C.F.; Bruno, I.J.; Chisholm, J.A.; Edgington, P.R.; McCabe, P.; Pidcock, E.; Rodriguez-Monge, L.; Taylor, R.; van de Streek, J.; Wood, P.A. *Mercury CSD 2.0*—New features for the visualization and investigation of crystal structures. *J. Appl. Crystallogr.* **2008**, *41*, 466–470. [[CrossRef](#)]
48. *STARe Software V14.00*, Mettler-Toledo AG: Columbus, OH, USA, 1992–2014.
49. Juribašić, M.; Bregović, N.; Stilinović, V.; Tomišić, V.; Cindrić, M.; Šket, P.; Plavec, J.; Rubčić, M.; Užarević, K. Supramolecular Stabilization of Metastable Tautomers in Solution and the Solid State. *Chem. A Eur. J.* **2014**, *20*, 17333–17345. [[CrossRef](#)] [[PubMed](#)]



© 2017 by the authors; licensee MDPI, Basel, Switzerland. This article is an open access article distributed under the terms and conditions of the Creative Commons Attribution (CC-BY) license (<http://creativecommons.org/licenses/by/4.0/>).